A Novel, Real-Time, In Vivo Mouse Retinal Imaging System

Mark C. Butler[1,2] and Jack M. Sullivan[1–6]

[1]Research Service, VA Western New York Healthcare System, Buffalo, New York, United States
[2]Department of Ophthalmology, Ross Eye Institute, University at Buffalo–SUNY, Buffalo, New York, United States
[3]Department of Pharmacology/Toxicology, University at Buffalo–SUNY, Buffalo, New York, United States
[4]Department of Physiology/Biophysics, University at Buffalo–SUNY, Buffalo, New York, United States
[5]Neuroscience Program, University at Buffalo–SUNY, Buffalo, New York, United States
[6]The SUNY Eye Institute, SUNY, University at Buffalo, Buffalo, New York, United States

Correspondence: Jack M. Sullivan, Departments of Ophthalmology, Pharmacology/Toxicology, and Physiology/Biophysics, University at Buffalo, The Ross Eye Institute, Veterans Administration Western New York Healthcare System Medical Research, Building 20, Room 245, 3495 Bailey Avenue, Buffalo, NY 14215, USA; js354@buffalo.edu, jackmsullivanmdphd@yahoo.com.

Submitted: December 31, 2014
Accepted: September 15, 2015

Citation: Butler MC, Sullivan JM. A novel, real-time, in vivo mouse retinal imaging system. *Invest Ophthalmol Vis Sci*. 2015;56:7159–7168. DOI:10.1167/iovs.14-16370

Purpose. To develop an efficient, low-cost instrument for robust real-time imaging of the mouse retina in vivo, and assess system capabilities by evaluating various animal models.

Methods. Following multiple disappointing attempts to visualize the mouse retina during a subretinal injection using commercially available systems, we identified the key limitation to be inadequate illumination due to off axis illumination and poor optical train optimization. Therefore, we designed a paraxial illumination system for Greenough-type stereo dissecting microscope incorporating an optimized optical launch and an efficiently coupled fiber optic delivery system. Excitation and emission filters control spectral bandwidth. A color coupled-charged device (CCD) camera is coupled to the microscope for image capture. Although, field of view (FOV) is constrained by the small pupil aperture, the high optical power of the mouse eye, and the long working distance (needed for surgical manipulations), these limitations can be compensated by eye positioning in order to observe the entire retina.

Results. The retinal imaging system delivers an adjustable narrow beam to the dilated pupil with minimal vignetting. The optic nerve, vasculature, and posterior pole are crisply visualized and the entire retina can be observed through eye positioning. Normal and degenerative retinal phenotypes can be followed over time. Subretinal or intraocular injection procedures are followed in real time. Real-time, intravenous fluorescein angiography for the live mouse has been achieved.

Conclusions. A novel device is established for real-time viewing and image capture of the small animal retina during subretinal injections for preclinical gene therapy studies.

Keywords: angiography, aperture, cornea, far-red, fluorescein, fundus, gene, Greenough, illumination, imaging, injection, in vivo, lens, microscope, mouse, novel, on-axis, optic nerve, paraxial, parafocal, photography, preclinical, pupil, real-time, retina, subretinal, therapy, vasculature

Novel gene therapy approaches for the eye are commonly tested initially in mouse or rodent models of disease.[1–8] Most studies currently use some form of recombinant adeno-associated virus (AAV) or lentiviral vector to deliver genetic constructs to the retina or other regions of the eye. Delivery of wild-type genetic expression constructs is a first line approach to testing gene-based therapies for autosomal recessive conditions.[3–6] More recently, posttranscriptional gene silencing agents as candidate therapeutics are being tested for treatment of autosomal dominant conditions in rodent models of disease.[2,9] A popular delivery route for vectors for retinal gene therapy is by way of subretinal injection,[6–8] which opens the subretinal space (separating outer segments of photoreceptors from the apical microvilli of the RPE) to permit efficient transduction of photoreceptors and/or RPE cells.[10] Use of off-axis illumination common in standard clinical surgical microscopes poorly satisfy the entrance numerical aperture of the small mouse eye (diameter ~3 mm) with a small dilated pupil aperture (≈1 mm), which makes it difficult to deliver robust input energy to the retinal surface to achieve quality specular imaging. Hence, vector delivery is often performed without direct or immediate visual feedback, and success and extent of delivery is often assessed on the basis of crude optical changes of the retinal red reflex, without clear delineation of the position of a subretinal fluid bleb, or post hoc through tissue expression analysis (e.g., enhanced green fluorescent protein [EGFP]).

We considered and tried various commercial systems for mouse eye imaging. A critical factor in efficient imaging is the delivery of light through the pupil to illuminate the intraocular contents. The small size of the mouse eye and tiny dilated pupil constrain design of a microscope with a large working distance, to allow surgical manipulations, while viewing the retina by high-quality imaging. Prior, long-working distance systems used human surgical microscopes or microscopes with ring lights, which all use off-axis spatially broad sources that cannot be efficiently collected in order to deliver condensed light energy into the small mouse pupil (Supplementary Fig. S1). Imaging systems that contact the surface of the eye (e.g., Micron IV; Phoenix Research Labs, Pleasanton, CA, USA), limit approaches for real-time surgical intervention (e.g., subretinal injections). Here, we designed and tested a long working distance, stereo

microscope–based, optical system that couples input light as a broad band or band-limited small spatial cone of illumination on-axis into the dilated mouse pupil. We call this device a retinal imaging system (RIS). We successfully used this system in both neonatal and adult mice in vivo to accomplish: (1) real time subretinal and intravitreal injections in the neonatal mouse eye, (2) imaging of normal and degenerative mouse retinas, (3) visualization of AAV-transduced regions of mouse retina, (4) far-red viewing of the mouse retina (to avoid light damage), and (5) true real-time intravenous fluorescein angiography in the live mouse. This inexpensive, long working distance device with constant illumination allows real-time surgical intervention and imaging of the retina or anterior segment of the eye, and rivals the imaging properties of commercially available contact imaging tools for the rodent eye.

A preliminary version of these results were presented in abstract/poster format (Butler MC, et al. *IOVS* 2010;51:ARVO E-abstract 3103).

Materials and Methods

Mouse Ocular Imaging System

The imaging system exploits a modified Greenough type stereo microscope (Stemi 2000-C; Zeiss, Thornwood, NY, USA). The illumination system launch is based upon a Xenon (Arc) 100-W lamp, 350 lumen output (6000°K color temperature), and a source optical numerical aperture (NA) = 0.52, which emits broad-band energy (CL-100 surgical Illuminator, Welch Allyn, Skaneateles Falls, NY, USA). Lamp output is coupled through a spherical mirror onto the face of a small core diameter (1.4-mm Single Fiber Illumination microlink headlight fiber) fiber optic launch that delivers optical energy to an application-specific optical train (see Results) to generate a narrow cone of light that is focused, after reflection off a small front surface angled mirror/prism (45°) into a small diameter circular spot (1.0–2.0 mm, variable spot size) at the dilated pupil aperture of the mouse eye. The focal point is 76 mm, at the lowest magnification, from the last optical element of the system and offers this working distance and good clearance for diverse surgical manipulations. While the 45° prism/mirror was fixed in the prototype design, in principle the prism could be rotated to steer the position of the beam within the pupil aperture. Engineered into the optical train are positions for multiple fluorescence excitation and emission band pass filters (Chroma, Omega, Semrock), which can easily convert the bright field imaging system into a fluorescence imaging device. A SPOT Flex pixel shifting color mosaic digital camera Model FX 15.2 (Diagnostics Instruments, Inc., Sterling Heights, MI, USA) was coupled onto the microscope platform and camera-specific software (SPOT software 4.6; Diagnostic Instruments, Inc.) acquired and processed images on a DELL desktop computer running Windows XP professional 2002 (Microsoft, Redmond, WA, USA).

Mouse Models

Animals lines used for imaging included the C57BL/6N (Charles River, Wilmington, MA, USA), C57BL/6J (Jackson Labs, Bar Harbor, ME, USA), a partially humanized mouse adRP model (C1xBL6) with a single dose of the C1 transgene of hRho P347S on the mouse Rho wild-type background.[11,12] The A1 mouse line is homozygous for the A1 transgene of hRho P347S on the mouse Rho knockout background.[11–14] A mouse model was developed which is homozygous for wild-type human Rho transgene (NHR-E)[15] on the mouse Rho knockout background (2HRho//1T1T) and has wild-type photoreceptor properties. A mouse Rho knockout model of retinal degeneration (129R-)[11] was also imaged. Animals were maintained in the Veterinary Medical Unit (VMU) at the Veterans Administration of Western New York Healthcare System (New York, NY, USA) under protocols reviewed and approved by the Institutional Animal Care and Use Committees (IACUC) at both the VA and the University at Buffalo (Buffalo, NY, USA). Animal use was in adherence with the ARVO Statement for the Use of Animals in Ophthalmic and Vision Research.

Anesthesia and Other Medications

Avertin was prepared as an aqueous solution of 2,2,2-tribromethanol (12.5 mg/mL) and tert-amyl alcohol (25 mg/mL; both Sigma-Aldrich Corp., St. Louis, MO, USA) with final adjusted pH 7.25 and filtered sterilized (0.22 μm; Millipore, Billerica, MA, USA) prior to dark storage of aliquots at −20°C.[16] Animals were anesthetized with 25 μL/gram of body mass via intraperitoneal (IP) injection. Eyes were topically anesthetized with Proparacaine hydrochloride (0.5% wt/vol; SANDOZ, Inc., Princeton, NJ, USA) and pupils dilated with one drop of Cyclopentolate hydrochloride (1% wt/vol; Bausch & Lomb, Inc., Tampa, FL, USA) and one drop of atropine sulfate (1% wt/vol; AKORN, Inc., Lakeforest, IL, USA). After injections eyes were coated with gentamicin sulfate ophthalmic ointment (0.3%, 3 mg/gram gentamicin base; Perrigo, Minneapolis, MN, USA). Buprenorphine hydrochloride (0.05 μg/gram, IP injection; Rickitt Benckiser Pharmaceuticals, Richmond, VA, USA) was given as needed for pain.

scAAV2/8-EGFP Packaging

A self-complementary AAV2 genome plasmid that contained an EGFP cDNA controlled by a CMV promoter was used to test for transduction in the mouse retina. The AAV plasmid was a gift of the Vector Core at the University of North Carolina (Chapel Hill, NC, USA). Vector was pseudotype-packaged into wild type AAV capsid 8 to titers greater than 10^{12} vector genomes/mL by University of North Carolina Vector Core. The viral prep used in these studies is specified (#3412).

Imaging Gel

A gel formulated from 2 mg/mL (wt/vol) high molecular weight (4×10^6 g/mole) carbomer in sterile 1X Dulbecco's PBS (Invitrogen, Grand Island, NY, USA) was used to form the viscous optically transparent interface between the mouse cornea and a premium cover glass (18 × 18 mm; Fisher Scientific, Pittsburgh, PA, USA). This combination of gel and glass cover slip suppress the strong optical front surface curvature of the mouse cornea and related spherical aberrations, to effectively create a Hruby-type lens (plano-concave) for enhanced retinal imaging.[17]

Intraocular and Subretinal Injections

Subretinal and intraocular injections were performed using sterilized glass micro needles. (capillary tubes 1.5-mm external diameter, 0.86-mm internal diameter, 100-mm length, Kimax-51; Kimble Glass Co., Chicago, IL, USA) fashioned on a P-97 Flaming/Brown micropipette puller (Sutter Instrument Co., Novato, CA, USA). Glass needles were back-filled with injection solution and mounted into an airtight electrode holder on a MMN-33 micro manipulator (Narishige, Long Island, NY, USA). The electrode holder was connected to a controlled pressure delivery device (PLI-100 micro injector; Harvard Apparatus, Boston, MA, USA). The needle was directed in a transscleral,

Investigative Ophthalmology & Visual Science

transchoroidal approach for subretinal injections, or a pars plana approach for intravitreal injections. The needle was directed 1 to 1.5 mm posterior to the corneal limbus in the nasal quadrant for subretinal injections. The needle is advanced until the tip is directly visualized in proximity of the subretinal space of the mouse eye, or at the boundary of retina and RPE. This is facilitated by the presence of fluorescein (0.5 mg/mL) within the injection pipette seen in contrast to the melanin pigment of the RPE. Once the glass needle is positioned, the fluid is delivered by the pressure injector (activated by foot pedal, 60 PSI at primary regulator/and 1–5 PSI at the needle tip) to force a small volume (~1 μL) of solution into the eye over a few seconds. Subretinal injections from the superior or inferior quadrant are also feasible. Successful subretinal injections are confirmed by high-resolution optical coherence tomography (OCT; Bioptigen, Morrisville, NC, USA). Mice were maintained at 37°C through the duration of the procedure using a heated water pad coupled to a water pump (Model RTE-140; NESLAB, Portsmouth, NH, USA).

Fluorescein Angiography

Fluorescein Lite 25% (250 mg/mL; ALTAIRE Pharmaceuticals, Aquebogue, NY, USA), diluted with sterile 1 × DPBS (final concentration 10 mg/mL; Gibco Life Technologies, Grand Island, NY, USA) was administered by bolus injection (50 μL) into the tail vein of anesthetized mice, positioned on the RIS imaging platform, through a 30-G stainless steel hypodermic needle. Spectral band pass filters appropriate for fluorescein (excitation = 482 nm/35 nm, Full Width Half Maximum [FWHM] = 39 nm); emission = 530 nm/525 nm cut-on wavelength longpass filter; Omega Optical, Brattleboro, VT, USA) were used to excite and capture fluorescence emission for imaging real-time fluorescein angiography. Far-red imaging was accomplished by introducing an excitation filter (692 nm/bp = 40 nm, FWHM = 47.6 nm) into the input light path.

Results

Optical System Design

The RIS is a cost-effective instrument designed to achieve optimal illumination of the mouse retina with broad band or band-limited stimuli for bright-field, far-red, or fluorescence imaging. The design requirements for the RIS included a long working distance for surgical manipulations (~8 cm), and on-axis (coaxial) illumination into the numerical aperture of the mouse pupil without overfilling the pupil, while maintaining field-of-view and depth-of-field of the standard Greenough-type stereo microscope.

The optical design schematic shows the overall system integration modeled on a Zeiss Stemi 2000-C microscope (Fig. 1A). An innovative feature of the system is that input light is delivered on-axis in the open optical "space" between the independent stereo view axes of the microscope. Fluorescence excitation or far-red input is shaped spectrally with interference filters. Fluorescence emission bandpass filters are placed proximal to the integrated camera. The microscope focus and magnification adjustments are not affected by RIS optics. The input source is based on a short arc, continuous xenon lamp, positioned adjacent to a spherical mirror that captures part of the energy and condenses it into the small diameter fiber optic cable (1.4 mm diameter NA ≈ 0.5; Fig. 1B). The spectral output of the lamp provides a relatively uniform broad band light source from 400 to 700 nm with a power of approximately 1 mWatts/cm^2 (Supplementary Fig. S2). This broad band source allows for a wide variety of different fluors to be imaged and even far-red imaging to be accomplished, simply by choosing the proper filter or filter sets. The fiberoptic launch couples to the microscope through an optical train of three achromatic lenses (two fixed positive lenses and a mobile negative lens, which capture energy from the fiber, shape the beam, and condense the beam into the specimen plane where the eye (NA ≈ 0.5) is positioned. A photograph of the prototype RIS system is shown (Fig. 1C). The optical train shapes the spot size of the beam to avoid overfilling the pupil and provide efficient energy transfer of light from the illuminator to the mouse pupil. The outcome of the RIS design optical train results in a narrow beam focused onto the dilated pupil plane with an adjustable spot size ranging from 1 to 2 mm through modulation of just one optical element (Fig. 1D). During practical imaging the application of an optical gel covered with a coverslip effectively removes the optics of the steep curvature of the anterior surface from the imaging challenge and also minimizes spherical aberrations of the small mouse eye to improve image quality, in principle, simulating the function of a commonly used Hruby lens[17] (Supplementary Fig. S3).

Major ergonomic features of RIS are the long working distance for surgical manipulations, simple conversions from bright field to far-red and fluorescence modes through rapid positioning of rails for excitation (2 or more positions) and emission (4 or more positions) filters, and an adjustable camera mount to make the ocular and camera's coupled-charged device (CCD) chip image planes para focal. Several features are novel in the RIS. First, the RIS is a noncontact system with approximately 8 cm of working distance between the last optical element and the eye as needed for surgical manipulation (e.g., placement of glass needles by micromanipulators). This positively differentiates our system from any contact based imaging system (e.g., Micron IV). The longer working distance is forced by the choice of an inexpensive stereo Greenough-type microscope, which narrows the angular field of view (FOV). Second, the illuminating light source, the fiber optic cable, and the optical element train were chosen to shape and focus a narrow intense beam of light, on optical axis, into the tiny dilated pupil to illuminate intraocular contents and achieve bright field, narrow field, or fluorescence imaging. This was the most severe optical design challenge. A commercial (endoscopic) light source was used to launch into a small core high NA fiberoptic and provided intense broad band spectral input for the system design. The numerical aperture or light collecting capacity of the mouse eye is surprisingly high (NA ~0.5, total angle ~ 60°) compared with the human eye (NA ~ 0.2, total angle: 23°).[18] In the ideal world we would have tried to match the optical delivery system NA to the NA of the eye but the long working distance precluded this option. Instead, we designed a lower NA delivery system that efficiently captures the fiber output energy and projects it into a narrow beam that can just fill the dilated pupil aperture. The narrow beam is shaped by the movement of a single negative lens (NA: 0.113–0.131, total angle = 13.0°–15.0°) and has a minimum spot size diameter of approximately 1.0 mm, which just fills the dilated pupil and avoids overfilling (vignetting). Third, we achieved on-axis illumination of the eye by exploiting unused optical "space," which exists between the independent view paths of the Greenough device. We centered a mirror to reflect the condensed illumination beam directly on optical axis with the mouse eye and pupil aperture. We can focus, modulate, and direct the illumination beam on-axis through the small pupil aperture of the mouse eye. This efficient designs allows on-axis spectral Maxwellian illumination of the interior of the mouse eye and is paramount to the use and achievement of our device to obtain superb images with simple operation at significantly lower cost relative to commercial devices (e.g., Micron IV).

Investigative Ophthalmology & Visual Science

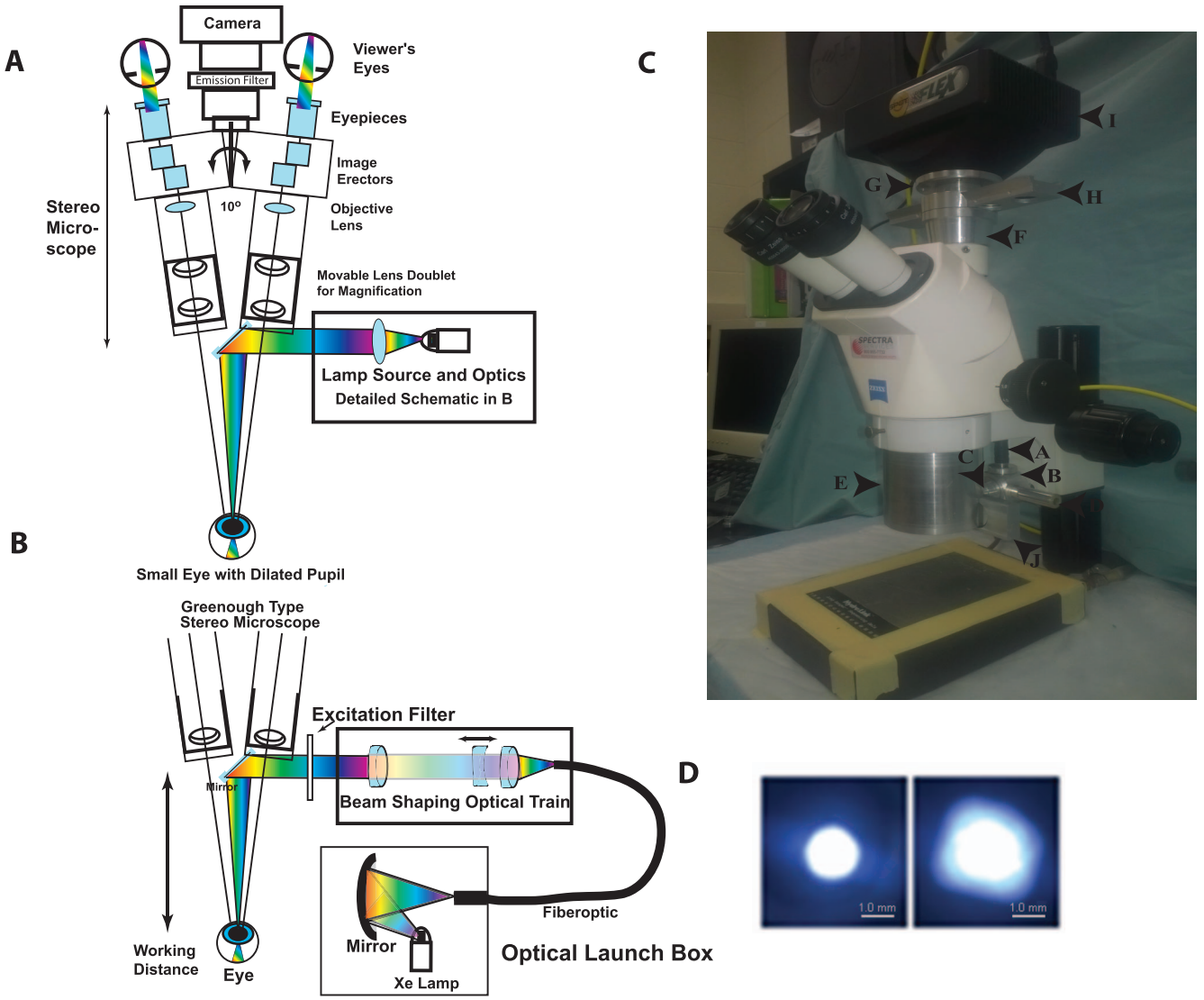

Figure 1. Schematic diagram of the major components of the on-axis retinal imaging platform. (**A**) An intense small gap continuous xenon source is collected and condensed into a small core diameter fiber optic with approximately matching numerical aperture. The fiber leaves the launch box and is coupled into the Greenough type stereo microscope exploiting the open optical "space" (~10°) between the two stereo viewing axes. The cone of light emerging from the fiber is collected, shaped, and condensed into a beam focus by an optical train of three achromatic lenses (two fixed positive lenses and one mobile negative lens) with the focal point approximately 7.5 cm from the last optical component in the system. The narrow condensed beam is folded onto the optical axis of the microscope by a tiny front surface mirror or prism that can be used to steer the beam. The beam condenses into the small dilated pupil of the mouse eye in a Maxwellian imaging paradigm. The mouse and eye are positioned to match this point in space for maximal coupling. The eye is visualized with a stereo imaging system and a camera is attached for photodocumentation. Excitation and emission filters are appropriately placed to modulate the input and output beams. (**B**) Optical schematic of the fiber optic launch box (Welch Allyn, CL-100) and the optical delivery train at the level of the microscope. The short arc xenon source with an NA 0.52 is coupled into a matched high NA fiber with a spherical mirror positioned proximate to the xenon lamp, which is held in a vertical position. The fiberoptic transmits the energy to the stereo microscope, initially orthogonal to the optical axis. An optical rail made from three achromatic lenses collects the energy from the fiber into an approximately collimated beam, shapes the angle of the beam (with the moveable negative achromatic lens), and condenses the beam into the specimen plane. The position of the fiber relative to the first positive achromatic lens shapes the collimation of the beam. The final positive lens focuses the energy onto the specimen plane. An excitation filter modulates the spectral pattern of the beam. A 45° mirror directs the beam onto the optical axis, which resides between the independent stereo imaging axes. (**C**) Image of the Zeiss Stemi 2000-C microscope modifications for the RIS converting it to the brightfield, far-red, and fluorescence setup. The components include the: fiber optic cable entry point (**a**), the fiber optic holder (**b**), the optical elements holder (**c**), the spot size regulator (**d**), the microscope body (**e**), the microscope/camera coupling spacer with emission filter rail (**f**), the adjustable z-axis camera mounting ring (**g**), the emission filter rail (four filters) (**h**), the SPOT Flex camera (**i**), and the excitation filter rail (**j**) (the CL-100 light source is not shown). (**D**) Spot sizes in the mouse pupil plane. Image of the minimum (*left*) and maximum (*right*) spot sizes created with a 1.4-mm core fiber input. Images were taken with the beam focused onto a flat optical surface placed at the focal point of the eye input beam. The spot size is controlled by moving the position of the negative beam shaping lens in the optical train. *Scale bars*: is 1.0 mm.

Investigative Ophthalmology & Visual Science

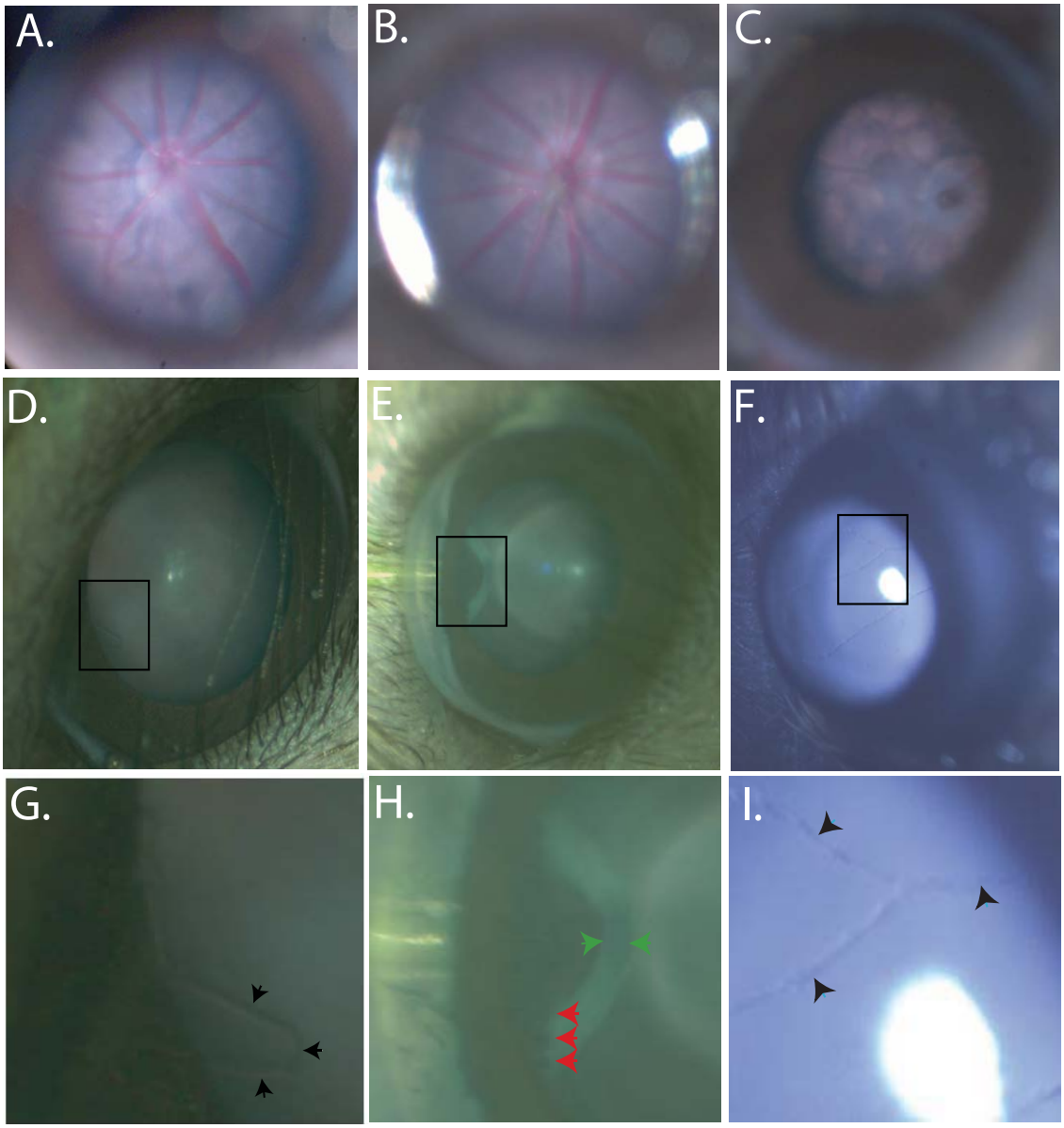

Figure 2. Bright field in vivo images demonstrating the RIS depth of field and imaging capabilities. Representative fundus images of a C57BL6(N) (6 months) (**A**), A wild-type human *RHO* on the mouse *RHO* knockout background (2HRho//1T/1T; ~4 months of age) (**B**); Mouse *RHO* knockout (129R-; ~4 months of age). (**C**) Regions of interest, demonstrating depth of field of the RIS, are *boxed* in images (**D–F**) are expanded in images (**G–I**) respectively, and show fine anatomical structures which can be identified. Images were enhanced for contrast and brightness to improve the fine details in images (**A**, **B**, **G**, **I**). Images from an A1 mouse (~1 month of age) of the anterior chamber, both the cornea and iris are clearly visible, even the smallest of blood vessels are visible protruding from the edge of the iris (*black arrow heads*) (**D**, **G**). The pars plana can be imaged with scleral depression allowing visualization of ciliary body processes (*red arrow heads*) and the retinal thickness can be visualized highlighted by the (*green arrow heads*) (**E**, **H**). Visualization of the hyaloid vessels (*black arrow heads*) is shown in (**F**, **I**) in a C57BL6(N); ~2-week old). Imaging of the mouse retina including optic nerve head and vasculature and retinal pigmentation can be clearly visualized (**A–C**). These images demonstrate the depth of view of the internal contents of the mouse eye provided by the RIS and the resolution capabilities of this system. The field of view allows the entire cornea to be imaged, but is more limited when imaging the retina due to the small diameter of the dilated mouse pupil, the effects of the mouse lenticular optics, and the long working distance of the instrument. Imaging of the entire retinal surface can be accomplished by manipulation of the eye or animal.

Operational Performance of the RIS

The capabilities of this device were first tested by examining the fundus of normal mice, transgenic mice, and mice with retinal degenerations (Figs. 2A–C). The device can be used to follow the time course of retinal degenerations in mice and provide photo documentation. Changes in the appearance of the retina and RPE are readily visualized with the RIS and anatomical differences in the optic nerve head and vasculature are obvious when comparing wild-type C57BL/6 animals to transgenic lines, which are known to develop retinal degenerations. In addition, the RIS is capable of imaging the cornea, anterior chamber, iris, lens, and the entire retina (including the pars plana region) by simple positioning of the mouse eye (rotation of eye or animal) relative to the input beam axis (Figs. 2D–I). The device is especially useful in efforts to develop surgical skills for subretinal and intravitreal injection of vector-containing fluids into the mouse eye for preclinical gene therapy studies. Using the RIS we have the ability to visualize

Investigative Ophthalmology & Visual Science

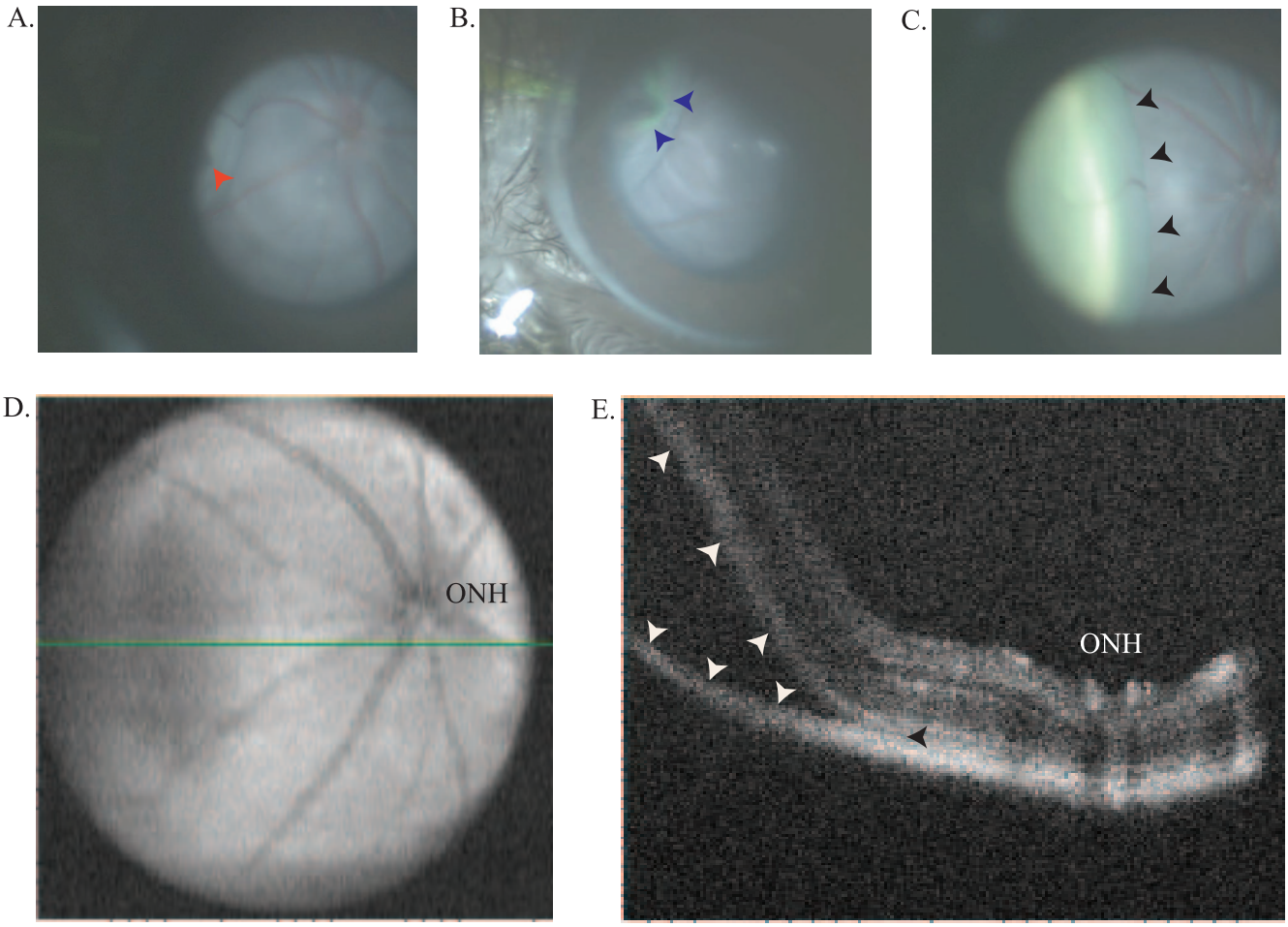

Figure 3. Subretinal injection imaged in real time. Initial, early, and final images of a subretinal injection in a C1xBL/6 mouse (~1.5 months of age) using a fluorescein sulfate in 1X PBS (ALTAIRE Pharmaceuticals, Inc.) to visualize the progression of the sub retinal bleb. A 10-second injection (16.6 PSI, using pulled glass capillary needle with a 2-µm tip diameter) captures the entire injection in real time. Including needle tip placement prior to RPE penetration (*red arrow*) (**A**), immediately following start of sub retinal injection (*blue arrows*) (**B**). Finally, the retinal detachment involving approximately 20% of total retina (*black arrows*) (**C**). Optical coherence tomography enface and B-scan images image of the subretinal injection site confirming the injection is located in the subretinal space of the retina. The enface image demonstrates the extent of the subretinal bleb identified by the hypo reflective region of the retina in the nasal region (*left side of image*) and the B-scan location in (**E**) is highlighted with a *green line* (**D**). A B-scan proximal to the optic nerve head (ONH) and including the leading edge of the injection bleb highlighted by the (*white arrows*) confirming the injection was localized to the sub retinal space identified by the (*black arrowhead*) (**E**).

the entire process of a subretinal injection, when done through a trans-scleral, transchoroidal approach, including placement of the needle (Fig. 3A) into the subretinal space and progression of the injection in real time (Fig. 3B [initial], Fig. 3C [final]). Optical coherence tomography imaging confirms the injection is in the subretinal space by the en-face (Fig. 3D) and b-scan (Fig. 3E) images. Subretinal injections via the trans-scleral, transchoroidal approach using fashioned glass micro needles placed under micromanipulator control avoid damage to the cornea, lens, lens zonules, ciliary body, and retina (retinotomy), and decreased the number of choroidal hemorrhages and cataracts observed in other approaches. The fluorescence imaging capabilities of the device have been used to identify regions within the retina in vivo that were successfully transduced by subretinal injected AAV-EGFP vector (Figs. 4A, 4B). In addition, the RIS can image the retina under far-red illumination conditions, which will be useful for subretinal or intravitreal injections under conditions that minimize potential retinal light damage in mouse models, which are light sensitive (Fig. 4C). A comparison of subretinal and intravitreal injection is also shows as imaged with the RIS (Supplementary Fig. S4). Finally, the fluorescence capabilities of the device were used to conduct real time intravenous fluorescein angiography after pulse injection of fluorescein into the tail vein. In the normal adult C57BL/6 mouse the initial arterial and then the arteriovenous phases appear rapidly, the recirculation phase is achieved rapidly and iris perfusion and later lid skin perfusion become apparent (Fig. 5A). Images of the fully perfused retina with fluorescein show the detail of the vasculature achieved with the RIS and changes in blood flow between healthy (C57BL/6, Fig. 5B) and degenerating retinas (A1, Fig. 5C [5.5 months], Fig. 5D [1 year]).

Discussion

Capacity of the Retinal Imaging System

We achieved proof-of-principle in development of a relatively simple and inexpensive instrument that allows detailed bright-field, far-red, and fluorescence imaging of small animal retinas in vivo. We demonstrated the utility of the RIS to: (1) noninvasively monitor the fundus appearance of retinal degenerations over time in single mouse models, (2) guide and assess subretinal

Investigative Ophthalmology & Visual Science

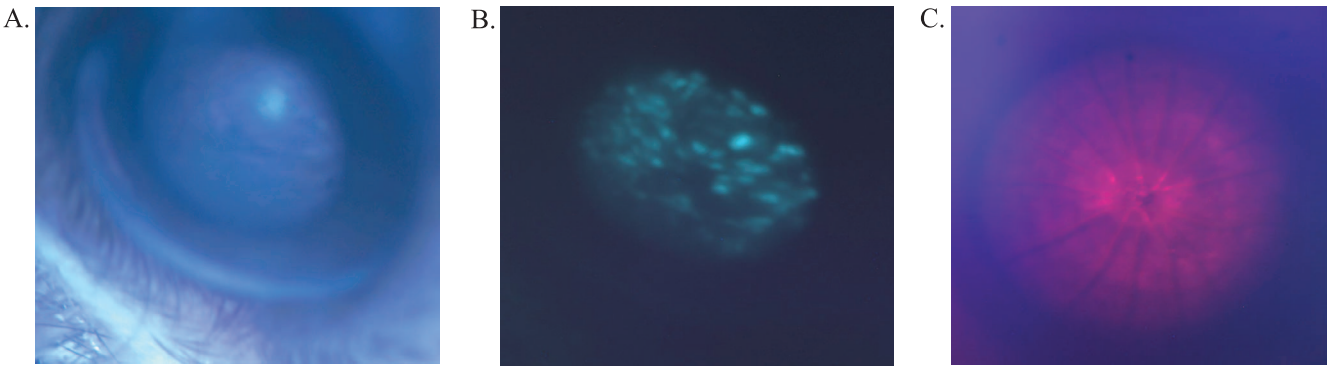

Figure 4. Bandpass limited imaging modes of the RIS for assessing subretinal injection efficiency and performing far red imaging. Enhanced green fluorescent protein expression assessed in vivo in the retina of a C1xC57BL/6 mouse that received a subretinal injection of AAV-EGFP virus (1.0 μL) at 14 days of age. The bright field (**A**) and fluorescence images (**B**) were taken 12 weeks post injection. Bandpass filters were used to excite the EGFP and capture its emission for fluorescence imaging. In vivo imaging of C1xBL6 mouse (~2 months of age) retina using a far red bandpass filter (692 nm peak, 40 nm bandpass) (**C**). This allows examination of the posterior pole and vasculature during dark-adapted studies or during subretinal injections in light sensitive animal models (to prevent light damage).

injections in preclinical gene therapy studies, (3) monitor extent of vector delivery and transduction (e.g., EGFP), and (4) conduct real time, true pulse intravenous fluorescein angiography in the live mouse.

Comparison With Other Types of Microscopes Used for Preclinical Gene Therapy Studies

In early retinal gene therapy studies for photoreceptors and RPE subretinal injections into small rodent eyes were conducted with available human surgical microscopes[19–25] and allowed only crude observation of changes in the optical appearance to assess extent of vector delivery. In all cases a corneal approach with stainless steel cannula was used for subretinal injection by hand guided delivery.[26] We examined two microscopes with off-axis illumination lamps having large filaments (several mm), that are effective in large human eyes with dilated pupils (9–10 mm) because they project sufficient light energy output into the eye to achieve sufficient intraocular illumination and allow real time imaging. In our hands, such microscopes were ineffective for retinal imaging because the illuminating light energy was not effectively coupled into the small dilated pupil of the mouse eye. Two of these prior studies mention the improved brightness of images with use of a halogen light source placed into the epifluorescence apparatus of the microscope for through-objective illumination, when compared to alternative "coaxial" and ring light delivery systems, but details were not elaborated.[24,25] Some images reported in this work appear to be of

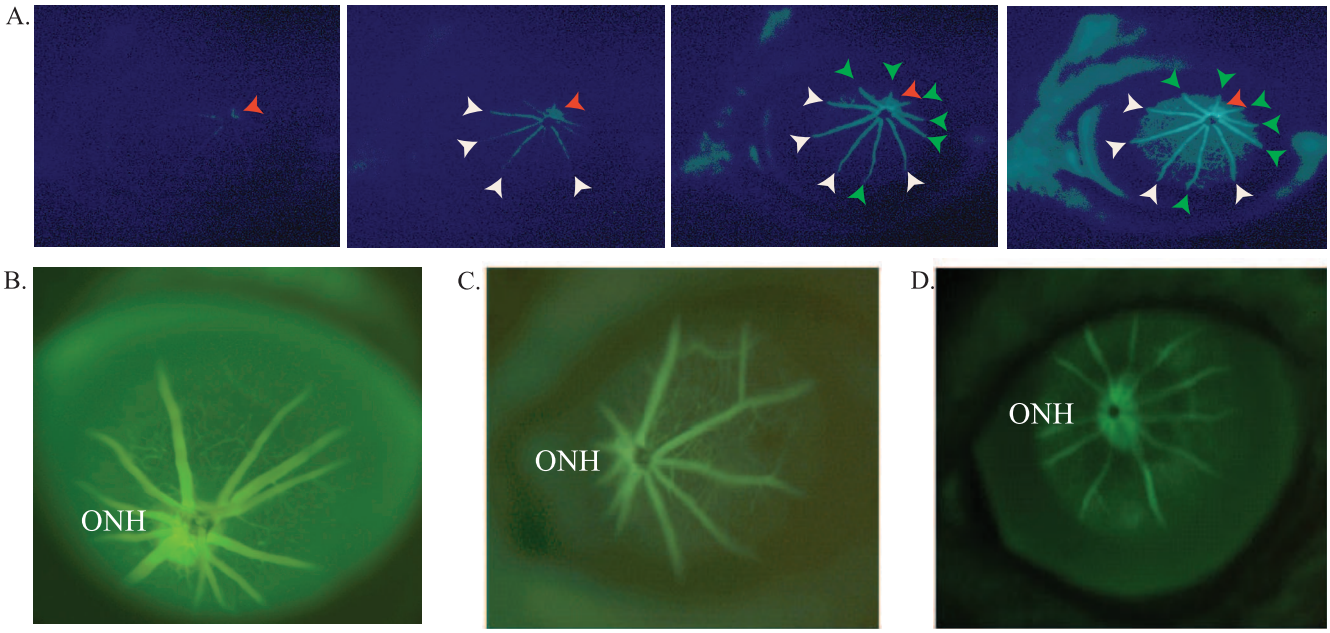

Figure 5. Images from in vivo fluorescein angiography in C1xBL/6 (~2 months old) in real time. Early, middle, and late images taken after administering a 50 μL bolus of 10 mg/mL fluorescein lite into the tail vein. The perfusion of the ONH (*red arrows*) is quickly followed by arterial vessels (*white arrows*), which is then followed by the arteriovenous phase (*green arrows*) then finally followed by visualization of the small vessels and capillary bed and finally general perfusion (**A**). Comparative intravenous fluorescein angiography (IVFA) of normal (C57BL6) and a degenerate retina in a homozygous P347S *RHO* (A1) retinal degeneration mouse. Intravenous fluorescein angiography of the A1 mouse retina shows poor perfusion through attenuated vasculature (due to progression of the retinal degeneration) (compare [**C**], 5.5 months and [**D**], 1 year). The brightness and contrast were modified to enhance the image details (**A**, **D**).

Investigative Ophthalmology & Visual Science

similar quality to those obtained on our system. The effectiveness of the RIS is demonstrated by our ability to successfully deliver virus preparations to the subretinal space approximately 80% of the time as determined by OCT imaging with pulled glass microneedles. Although, existing microscopes were successfully used in prior studies using relatively large stainless steel needles and provided adequate images of the rodent fundus and visualization of injection blebs[26–28] a fine glass tip is significantly more challenging to visualize and its careful placement under direct visualization is responsible for our success. There is no comparable existing system that allows for continuous, adequate illumination, with significant working distance for necessary micromanipulators required for surgical manipulations of the mouse eye, at a reasonable price.

A review of recent literature yielded a number of papers, which presented fundus images from rat eyes.[26–28] A few papers included images of retinal detachments including pre- and postinjection images, however none clearly demonstrate the entire process of subretinal injection.[26,28,29] Many papers have images of both fundus and or fluorescein angiography (after IP injection) obtained with commercial and expensive Micron- or Scanning Laser Ophthalmoscope (SLO)-based instruments.[30–35] Although, these instruments provide comparable images to our device they cost approximately 10 times more than our system. The Micro-III or IV devices (Phoenix Research Labs) are cornea contact imaging devices with a 50° FOV that generate images of high quality.[35] However, contact device systems do not readily adapt for surgical manipulations. In Vivo Confocal Neuroimaging (ICON) has been used to visualize single ganglion cells in the retina with a confocal microscope and an adaptive biconcave lens placed on the cornea.[36] While excellent images may be obtained on this device the working distance with typical objective lenses severely constrains surgical adaptation. The SLO-based systems also provide excellent imaging capabilities of the mouse fundus, however, some constraints of SLO-based systems include monochromatic images, difficulties imaging mice less than 1 month of age due to the small size of the eye, and lack of control of certain light sources on SLO systems.[37] Other systems were also used in a few of the publications, including Topcon,[38,39] FLIO,[40] TEFI,[41] and Kowa[42,43] systems. These systems have inherent limitations for either monitoring real-time surgical techniques or providing adequate clearance for surgical equipment required for procedures like subretinal injections. Clinical ophthalmological imaging systems have also been used to image the mouse eye. A clinical fundus photography camera with a 20-diopter (D) lens placed in front of the mouse eye and was able to image the mouse fundus.[38,39] This is not a system that would lend itself to a real-time surgical microscope and the relative imaging capacity relative to our system is not known. A portable Kowa fundus camera and a 90-D field lens to obtain images of the fundus of various mouse genetic lines.[42,43] The Kowa fundus camera (e.g., Genesis D) uses a xenon flash illumination system for human fundus photo generation. The xenon flash offers a broad-band white light illumination but the lamp itself does not appear to be a narrow arc device. The system has variable intensity but initiates a single flash, and thus can be used only for single frame photography and not real-time imaging. The use of contact endoscopic fibers based on gradient index lenses allows small eye fundus imaging with high resolution but could not be readily adapted to surgical needs.[41] All of the above challenges of these expensive systems are remedied with the RIS providing full color images, on animals as young p14 with ease, complete control of light intensity and spot size to allow optimized illumination for imaging needs at a fraction of the cost of such systems. While the contact Micron IV device appears to use an on-axis source and has a wide NA (because it shrinks the working distance to zero), we achieve both a range of illumination conditions with equivalent visual resolution and with the surgical option at much less cost. The narrow input beam, because of internal reflectivity within the small mouse eye, does not limit viewing to only the region of direct illumination, so there is no constraint that emerges there.

Limitations and Potential Improvements of the RIS Device

A limitation of the RIS, given that it is a noncontact imaging device, is the FOV. At the lowest magnification and at the design working distance of the Stem-2000C (92 mm; without RIS attachments) the object field is 35.4 mm leading to a total FOV of approximately 22°. In contrast the FOV of the Micron IV contact device is 50°. The tradeoff of FOV in the RIS can be managed by positioning the eye relative to the beam axis to illuminate different retinal regions. Although, the FOV is approximately one-half the FOV of the Micron III or IV system, it was more than adequate for all our imaging requirements. The RIS was designed for real-time subretinal surgery on the mouse eye, whereas the Micro IV appears incapable of such adaptations. Also, while not a major limitation, the RIS, like the Micron IV, uses discrete filters for excitation/emission rather than a device with uniform control over spectral input/output for fluorescence. The RIS, like the Micron IV, uses continuous illumination. A flash input, such as in the Kowa fundus camera system, can delivery substantial energy (Joules) in a single flash that can potentially lead to brighter images. The continuous light source can also be modulated for intensity at the level of the CL-100 launch, and the image intensity can be modulated by controlling the exposure duration of the camera. Another advantage of a brief and bright flash coupled efficiently into the mouse eye is that the image acquisition is less affected by the breathing of the animal. One means of coupling a flash system to the RIS is to use established technology[44] in which a short arc xenon flash is coupled optically into a 1-mm core fiber optic of approximately 0.48 NA. The fiber from this system could immediately couple to the RIS and the microsecond flash system allows control over flash spectrum with 10 discrete filters on a filter wheel. Flash intensity in this system is regulated by controlling voltage on the flash capacitor.

Acknowledgments

The authors thank Janis Lem, PhD (Tufts New England Medical Center) for the gift of the C1 transgenic human P347S *RHO* line and the exon 1 mouse *RHO* knockout, G. Jane Farrar, PhD, and Peter Humphries, PhD (Trinity College, Dublin, IRE) for the gift of the NHR-E transgene model in the heterozygous state on the mouse exon 2 *RHO* knockout background, and Tiansen Li, PhD (then at Harvard Medical School) for the gift of the homozygous A1 transgenic human P347S *RHO* line on the mouse *RHO* knockout background. They thank Josh Wang, MD, and Sarah X. Zhang, MD, for the images of the C57BL/6J retinas taken on the Micro-III system that were shared for our comparisons (University at Buffalo, Ophthalmology Department). They also thank Steven J. Fliesler, PhD (Department of Ophthalmology, University at Buffalo) for the review of the manuscript.

Supported in part by National Eye Institutes/National Institutes of Health (NEI/NIH; Bethesda, MD, USA) R01 Grant EY013433 (JMS) and NEI/NIH R24 Grant EY016662 (UB Vision Infrastructure Center, PI: M Slaughter, Director- Biophotonics Module: JMS), Challenge and Unrestricted Grants to the Department of Ophthalmology/University at Buffalo from Research to Prevent Blindness (New York, NY, USA), and a grant (JMS) from the Oishei Foundation (Buffalo, NY, USA). Supported, in part, by a Veterans Administration Merit Award grant (1I01BX000669; JMS). The study was conducted at, and supported in part by, the Veterans

Administration Western New York Healthcare System. The contents do not represent the views of the Department of Veterans Affairs or the United States government.

Disclosure: **M.C. Butler**, None; **J.M. Sullivan**, None

References

1. Regus-Leidig H, Fuchs M, Lohner M, et al. In-vivo knockdown of Piccolino disrupts presynaptic ribbon morphology in mouse photoreceptor synapses. *Front Cell Neurosci*. 2014;8:1–13.
2. Jiang L, Frederick JM, Baehr W. RNA interference gene therapy in dominant retinitis pigmentosa and cone-rod dystrophy mouse models caused by GCAP1 mutations. *Front Mol Neurosci*. 2014;7:1–8.
3. Seo S, Mullins RF, Dumitrescu AV, et al. Subretinal gene therapy of mice with Bardet-Beidl Syndrome Type-1. *Invest Ophthalmol Vis Sci*. 2013;54:6118–6132.
4. Molday LL, Djajadi H, Yan P, et al. RD3 gene delivery restores guanylate cyclase localization and rescues photoreceptors in the RD3 mouse model of Leber congenital amaurosis 12. *Hum Mol Genet*. 2014;22:3894–3905.
5. Pang JJ, Lei L, Dia X, et al. AAV-mediated gene therapy in mouse models of recessive retinal degeneration. *Curr Mol Med*. 2012;12:316–330.
6. Vandenberghe LH, Auricchio A. Novel adeno-associated viral vectors for retinal gene therapies. *Gene Ther*. 2012;19:162–168.
7. Tenenbaum L, Lehtonen E, Monahan PE. Evaluation of risks related to the use of adeno-associated virus based vectors. *Curr Gene Ther*. 2003;3:545–565.
8. Bainbridge JW, Mistry AR, Thrasher AJ, Ali RR. Gene therapy for ocular angiogenesis. *Clin Sci (Lond)*. 2003;104:561–575.
9. Gorbatyuk M, Justilien V, Liu J, Hauswirth WW, Lewin AS. Preservation of photoreceptor morphology and function in P23H rats using an allele independent ribozyme. *Exp Eye Res*. 2007;84:44–52.
10. Igarashi T, Miyake K, Asakawa N, Miyake N, Shimada T, Takahashi H. Direct comparison of administration routes for AAV-8 mediated ocular gene therapy. *Curr Eye Res*. 2013;38:569–577.
11. Humphries MM, Rancourt D, Farrar GJ, et al. Retinopathy induced in mice by targeted disruption of the rhodopsin gene. *Nat Genet*. 1997;15:216–219.
12. Lem J, Krasnoperova NV, Calvert PD, et al. Morphological, physiological, and biochemical changes in rhodopsin knockout mice. *Proc Natl Acad Sci U S A*. 1999;96:736–741.
13. Li T, Snyder WK, Olsson JE, Dryja TP. Transgenic mice carrying the dominant rhodopsin mutation P347S: evidence for defective vectorial transport of rhodopsin to the outer segments. *Proc Natl Acad Sci U S A*. 1996;93:14176–14181.
14. Brill E, Malanson KM, Radu RA, et al. A novel form of transducin-dependent retinal degeneration: accelerated retinal degeneration in the absence of rod transducin. *Invest Ophthalmol Vis Sci*. 2007;48:5445–5453.
15. Olsson, JE, Gordon JW, Pawlyk BS, et al. Transgenic mice with a rhodopsin mutation (Pro23His): a mouse model of autosomal dominant retinitis pigmentosa. *Neuron*. 1992;9:815–830.
16. Papaioannou VE, Gox JG. Efficacy of tribromoethanol anesthesia in mice. *Lab Anim Sci*. 1993;43:189–192.
17. Hruby K. Clinical examination of the vitreous body. *Proc Roy Soc Med*. 1953;47:163–170.
18. Geng Y, Schery LA, Sharma R, et al. Optical properties of the mouse eye. *Biomed Opt Exp*. 2011;2:717–738.
19. Bennett J, Tanabe T, Sun D, et al. Photoreceptor cell rescue in retinal degeneration (*rd*) mice by in vivo gene therapy. *Nat Med*. 1996;2:649–654.
20. Bennett J, Duan D, Engelhardt JF, Maguire AM. Real-time noninvasive in vivo assessment of adeno-associated virus-mediated retinal transduction. *Invest Ophthalmol Vis Sci*. 1997;38:2857–2863.
21. Ali RR, Reichel MB, Thrasher AJ, et al. Gene transfer into the mouse retina mediated by an adeno-associated viral vector. *Hum Mol Genet*. 1996;5:591–594.
22. Rolling F, Shen W-Y, Tabarias H, et al. Evaluation of adeno-associated virus-mediated gene transfer into the rat retina by clinical fluorescence photography. *Hum Gene Ther*. 1999;10:641–648.
23. Johnson CJ, Berglin L, Chrenek MA, Redmond TM, Boatright JH, Nickerson JM. Technical brief: subretinal injection and electroporation into adult mouse eyes. *Mol Vis*. 2008;14:2211–2226.
24. Nickerson JM, Goodman P, Chrenek MA, et al. Subretinal delivery and electroporation in pigmented and nonpigmented adult mouse eyes. In: Shu-Zhen Wang, ed. *Retinal Development: Methods and Protocols, Methods in Molecular Biology*. Berlin, Germany: Springer Science+Business Media; 2012:53–69.
25. Nickerson JM, Getz SE, Sellers JT, et al. DNA delivery in adult mouse eyes: An update with corneal endothelium outcomes. *Methods Mol Biol*. 2014;1121:165–177.
26. Timmers AM, Zhang H, Squitieri A, Gonzalez-Pola C. Subretinal injections in rodent eyes: effects on electrophysiology and histology of rat retina. *Mol Vis*. 2000;7:131–137.
27. Zacks DN, Hanninen V, Pantcheva M, Ezra E, Grosskreutz C, Miller JW. Caspase activation in an experimental model of retinal detachment. *Invest Ophthalmol Vis Sci*. 2003;44:1262–1267.
28. Iliaki E, Poulaki V, Mitsiades N, Mitsiades CS, Miller JW, Gragoudas ES. Role of a4 integrin (CD49d) in the pathogenesis of diabetic retinopathy. *Invest Ophthalmol Vis Sci*. 2009;50:4898–4904.
29. Matsumoto H, Miller JW, Vavvas DG. Retinal detachment model in rodents by subretinal injection of sodium hyaluronate. *J Vis Exp*. 2013; 79:e50660.
30. Hasegawa E, Sweigard H, Husain D, et al. Characterization of a spontaneous retinal neovascular mouse model. *PLoS One*. 2014;9:1–8.
31. Song D, Zhao L, Li Y, et al. The oral iron chelator deferiprone protects against systemic iron overload–induced retinal degeneration in hepcidin knockout mice. *Invest Ophthalmol Vis Sci*. 2014;55:4525–4532.
32. Mao H, Seo SJ, Biswal MR, et al. Mitochondrial oxidative stress in the retinal pigment epithelium leads to localized retinal degeneration. *Invest Ophthalmol Vis Sci*. 2014;55:4613–4627.
33. Oczos J, Sutter I, Kloeckener-Gruissem B, et al. Lack of Paraoxonase 1 alters phospholipid composition, but not morphology and function of the mouse retina. *Invest Ophthalmol Vis Sci*. 2014;55:84714–84727.
34. Lockhart CM, Nakano M, Rettie AE, Kelly EJ. Generation and characterization of a murine model of Bietti crystalline dystrophy. *Invest Ophthalmol Vis Sci*. 2014;55:5572–5581.
35. Kim S, Yang H, Chang Y, et al. Deletion of aryl hydrocarbon receptor AHR in mice leads to subretinal accumulation of microglia and RPE atrophy. *Invest Ophthalmol Vis Sci*. 2014;55:6031–6040.
36. Sabel BA, Engelmann R Humphrey MF. In vivo confocal neuroimaging (ICON) of CNS neurons. *Nat Med*. 1997;2:244–247.

Investigative Ophthalmology & Visual Science

37. Paques M, Sionutti M, Roux MJ, et al. High Resolution fundus imaging by confocal scanning laser ophthalmoscopy in the mouse. *Vision Res*. 2006;46:1336–1345.
38. Ye F, Kaneko H, Nagasaka Y, et al. Plasma-activated medium suppresses choroidal neovascularization in mice: a new therapeutic concept for age-related macular degeneration. *Sci Rep*. 2015;5:7705.
39. DiLoreto D Jr, Grover DA, Del Cerro C, Del Cerro M. A new procedure for fundus photography and fluorescein angiography in small laboratory animal eyes. *Curr Eye Res*. 1994; 13:157–161.
40. Dysli C, Dysli M, Enzmann DV, Wolf S, Zinkernagel MS. Fluorescence lifetime imaging of the ocular fundus in mice. *Invest Ophthalmol Vis Sci*. 2014;55:7206–7215.
41. Paques M, Guyomard J-L, Simonutti M, et al. Panretinal, high resolution color photography of the mouse fundus. *Invest Ophthalmol Vis Sci*. 2007;48:2769–2774.
42. Hawes NL, Smith RS, Chang B, Davidson M, Heckenlively JR, John SWM. Mouse fundus photography and angiography: a catalog of normal and mutant phenotypes. *Mol Vis*. 1999;5:22.
43. Chang B, Hurd R, Wang J, Nishina P. Survey of common eye diseases in laboratory mouse strains. *Invest Ophthalmol Vis Sci*. 2013;54:4974–4981.
44. Sullivan JM. Low-cost, monochromatic, microsecond flash microbeam apparatus for single-cell photolysis of rhodopsin or other photolabile pigments. *Rev Sci Instrument*. 1998; 69:527–539.

Investigative Ophthalmology & Visual Science